

VERY HIGH ENERGY γ -RAY AFTERGLOW EMISSION OF NEARBY GAMMA-RAY BURSTS

R. R. XUE^{1,2}, P. H. TAM³, S. J. WAGNER³, B. BEHERA³, Y. Z. FAN^{4,1} AND D. M. WEI^{1,5}

¹ Purple Mountain Observatory, Chinese Academy of Sciences, Nanjing 210008, China.

² Graduate School, Chinese Academy of Sciences, Beijing, 100012, China.

³ Landessternwarte, Universität Heidelberg, Königstuhl, Germany.

⁴ Niels Bohr International Academy, Niels Bohr Institute, University of Copenhagen, Blegdamsvej 17, DK-2100 Copenhagen, Denmark.

⁵ Joint Center for Particle Nuclear Physics and Cosmology of Purple Mountain Observatory – Nanjing University, Nanjing 210008, China.

Draft version March 1, 2022

ABSTRACT

The synchrotron self-Compton (SSC) emission from Gamma-ray Burst (GRB) forward shock can extend to the very-high-energy (VHE; $E_\gamma > 100$ GeV) range. Such high energy photons are rare and are attenuated by the cosmic infrared background before reaching us. In this work, we discuss the prospect to detect these VHE photons using the current ground-based Cherenkov detectors. Our calculated results are consistent with the upper limits obtained with several Cherenkov detectors for GRB 030329, GRB 050509B, and GRB 060505 during the afterglow phase. For 5 bursts in our nearby GRB sample (except for GRB 030329), current ground-based Cherenkov detectors would not be expected to detect the modeled VHE signal. Only for those very bright and nearby bursts like GRB 030329, detection of VHE photons is possible under favorable observing conditions and a delayed observation time of $\lesssim 10$ hours.

Subject headings: Gamma Rays: bursts — ISM: jets and outflows — radiation mechanism: non-thermal

1. INTRODUCTION

On February 28, 1997, the first X-ray afterglow of a Gamma-ray burst (GRB) was detected, leading to the identification of its progenitor at cosmological distances (Costa et al. 1997). In a few days, the afterglow faded away with time as a power law. This behavior is satisfactorily explained in the spherical (isotropic) fireball model involving relativistic ejecta decelerated by circumburst medium (Mészáros & Rees 1997). The introduction of collimated jets relaxes the energy requirement of GRBs by a factor of several hundred, as well as explains the steeper temporal decay of afterglows (Rhoads 1999; Sari et al. 1999).

GRBs are extra-galactic sources of GeV and probably higher energy photons. Evidences of distinct high-energy component have been accumulated by EGRET onboard the Compton Gamma-Ray Observatory: (1) Hurley et al. (1994) reported the detection of long-duration MeV–GeV emission of GRB 940217 lasting up to 1.5 hour after the keV burst, including an ~ 18 GeV photon. This burst is the longest and the most energetic among those GRBs with detected high-energy emission so far; (2) González et al. (2003) revealed a high-energy component of GRB 941017 temporally and spectrally different from the low-energy component.

In the fireball model, synchrotron emission of shock-accelerated electrons is commonly thought to produce prompt γ -ray emission as well as afterglow emission at lower energies (e.g., Sari et al. 1998). It is natural to expect that these photons are inverse-Compton up-scattered by electrons, giving rise to a higher energy component peaking at sub-GeV to TeV energies (Wei & Lu 1998; Sari & Esin 2001). When electrons scatter the self-

emitting synchrotron photons, synchrotron self-Compton (SSC) emission is resulted. In the external shock scenario, the temporal profile of the SSC emission from forward shock electrons is similar to that of the low energy afterglow emission and no significant time lag is expected.

The *Swift* satellite, thanks to its rapid response time and accurate localization, has started a new era of research on GRBs. Different modifications to the standard afterglow model are put forward to explain the peculiar behaviors exhibited in the X-ray light curves, in particular the shallow declining phase (Zhang et al. 2006; Nousek et al. 2006). Recently, the SSC emission of the modified forward shock has been extensively discussed in the literature (Wei & Fan 2007; Gou & Mészáros 2007; Fan et al. 2008; Galli & Piro 2007; Yu et al. 2007) and applied to the case of GRB 940217 (Wei & Fan 2007).

The AGILE (Astro-rivelatore Gamma a Immagini L'Espresso) satellite, launched on April 23, 2007, is dedicated to high-energy γ -ray astronomy. The Fermi Gamma-ray Space Telescope (FGST) was launched on June 11, 2008. The Large Area Telescope (LAT) onboard covers the energy range from 20 MeV to 300 GeV and its effective area is about 5 times larger than that of EGRET at GeV energies. The first GRB observations with LAT have resulted in detection of photons with energies larger than ~ 1 GeV from several GRBs (Omodei 2008; Tajima et al. 2008). Dermer et al. (2000), Zhang & Mészáros (2001b), and Wang et al. (2001) predicted promising and detectable SSC emission from the forward shock with FGST out to $z \sim 1$.

Most of the discussions in the literature have focused on the afterglow emission from tens of MeV to GeV. LAT can also detect very-high-energy (VHE; > 100 GeV) afterglow emission. However, with a small effective

area $\sim 10^4 \text{ cm}^2$, it is very hard to have a significant detection at such high energy. Imaging atmospheric Cherenkov telescopes such as H.E.S.S.¹, MAGIC², and VERITAS³ may serve better at energies above $\sim 100 \text{ GeV}$ because of their much larger effective area ($\sim 10^8 - 10^9 \text{ cm}^2$) and a high rejection rate of hadronic background. The effective collecting area of Cherenkov telescopes increases with energy (Aharonian et al. 2006b). Some of these large area Cherenkov detectors have been used to set constraints on the possible VHE afterglow component of GRBs (Albert et al. 2007; Horan et al. 2007; Aharonian et al. 2009). It is thus desirable to see whether these results are consistent with the predictions of the fireball model. Our aim of this paper is also to investigate the prospect of significant detections in the future. To have a reliable estimate of the afterglow emission at energies above 100 GeV , one needs to calculate the forward shock emission (both synchrotron and SSC emission of the shocked electrons) carefully. The attenuation of VHE photons by the cosmic infrared background is also taken into account. Since the attenuation effect for photons with an energy $>100 \text{ GeV}$ is more severe for high-redshift GRBs, we limit our GRB sample to nearby events.

This paper is organized as follows: in §2, we describe the GRB afterglow model, introduce the code that is used in the afterglow modeling and the calculation of the SSC emission from GRB forward shock. In §3, we present the expected results of the SSC model using reasonable parameter values for GRBs. In §4, we describe the GRB sample which includes six nearby GRBs with sufficient multi-wavelength afterglow data and predict their corrected energy flux after the attenuation by the cosmic background during the afterglow phase, which is then compared with the available observational data. We summarize our results and discuss their implications in §5. We conclude in §6.

2. AFTERGLOW MODELING

2.1. GRB Afterglow Model

While synchrotron emission is widely considered to be responsible for the radio, optical, and X-ray afterglows (e.g. Sari et al. 1998), inverse Compton scattering of forward shock photons is considered in details by Wei & Lu (1998, 2000) and Sari & Esin (2001). Inverse Compton scattering may considerably change the temporal and spectral behavior of GRB afterglows, and its cooling effect on electrons accelerated in external shocks will contribute to the photon spectra at sub-GeV to TeV energy range (Mészáros & Rees 1994; Dermer et al. 2000; Zhang & Mészáros 2001b; Wang et al. 2001).

In the afterglow model, both synchrotron emission and inverse Compton emission are taken into account. It is assumed that: (1) the external medium is homogenous with a density n or a wind profile $n \propto R^{-2}$; (2) the relativistic jet is uniform, i.e. energy per solid angle is independent of direction within the jet; (3) the shock parameters (ϵ_e and ϵ_B , fractions of the shock energy given to the

electrons and the magnetic field, respectively) are constant; (4) the energy distribution of electrons accelerated in shocks follows $dN_e/dE \propto E^{-p}$; (5) the possible achromatic flattening in the afterglow light curve is due to energy injection in the form $E_k \propto t^{1-q}$ (Cohen & Piran 1999; Zhang & Mészáros 2001a) or $E_k \propto [1 + (t/T)^2]^{-1}$ with T being the initial spin-down time scale (Dai & Lu 1998).

The parameters involved in this afterglow model include: E_0 (the initial isotropic outflow energy), θ_0 (the initial half-angle of the jet), n (the density of the homogeneous external medium) or A (the wind parameter), p (the power-law index of energy distribution of shock-accelerated electrons), ϵ_e , and ϵ_B (shock parameters). In the case where energy injection is necessary, three additional parameters: L_{eje} (the injected luminosity in the rest frame), the timescale of energy injection and q , are included.

2.2. A Brief Description of the SSC Model

The code used in our afterglow modeling and the prediction of the SSC emission is that developed by Fan et al. (2008), who carry out numerical calculations of synchrotron and SSC emission of the external forward shock in the afterglow phase⁴. The reverse shock emission, predicted in the fireball model but not detected in most events (Roming et al. 2006; Rykoff et al. 2009), is not taken into account.

The key treatments (see §3 of Fan et al. 2008, for details) are as follows: (i) The dynamical evolution of the outflow is followed using the formulae in Huang et al. (2000), which describes the hydrodynamics in both relativistic and non-relativistic phases. (ii) The arbitrary assumption that the distribution of shocked electrons is always in a quasi-stationary state is considered to be unsatisfactory and the energy distribution of electrons is calculated by solving the continuity equation with the power-law source function $Q = K\gamma_e^{-p}$, normalized by a local injection rate (Moderski et al. 2000). (iii) The observed flux is integrated over the “equal-arrival surface”. (iv) The Klein-Nishina correction of the inverse Compton emission has been included. (v) Energy injection into the outflow is considered necessary in reproducing some multi-frequency afterglow data of some GRBs. This may change the dynamics significantly.

By fitting the low-energy multi-wavelength afterglows, from radio to X-ray band, parameters involved in the afterglow model are gotten. *Simultaneous afterglow data in at least two well-separated wavebands are needed to get a relatively well-constrained set of parameters.*

A rough estimate of the energy-integrated VHE afterglow flux (without correction by the cosmic background) is given by

$$F_{>100\text{GeV}} \propto \frac{(1+z)L_{\text{SSC}}}{D_L^2} \max\{(\nu_c^{\text{SSC}})^{\frac{p-2}{2}}, (\nu_m^{\text{SSC}})^{\frac{p-2}{2}}\} \quad (1)$$

where L_{SSC} is the total luminosity of the SSC emis-

⁴ The cooling of the forward shock electrons by the so-called “central engine afterglow” emission (the emission powered by the re-activity of the central engine in the afterglow phase, like the flares (e.g., Nousek et al. 2006) or the plateaus followed by a sudden drop (e.g., Zhang 2009)) and the corresponding inverse Compton emission can also be calculated self-consistently. But for our current sample people did not see such emission.

¹ <http://www.mpi-hd.mpg.de/hfm/H.E.S.S./H.E.S.S..html>

² <http://www.magic.mppmu.mpg.de/>

³ <http://veritas.sao.arizona.edu/>

sion (see eq.(23-27) in Fan et al. 2008, for the expression), ν_m^{SSC} and ν_c^{SSC} are the typical SSC emission frequency and the SSC cooling frequency of the forward shock electrons (see eq.(33-34) in Fan et al. 2008, the case of $k = 0$, for the expressions) and D_L is the luminosity distance of the event.

3. MODEL PREDICTION

High energy photons, especially those in the TeV range, will be attenuated by the cosmic background light. Various models of the spectral energy distribution of the cosmic infrared background are proposed (Primack et al. 2001; Totani & Takeuchi 2002; Kneiske et al. 2002; Stecker et al. 2006), but all these models give comparable opacities for low redshifts. In this work, a level consistent with a study of two distant blazars and galaxy counts is used (P0.45, Aharonian et al. 2006a).

We adopt reasonable values of parameters for nearby GRBs and predict the spectra in high-energy to VHE range. After corrected for the attenuation by extragalactic background, we compare them with the sensitivity levels of γ -ray instruments.

Parameters assumed and the time-averaged spectra, including both synchrotron and SSC components from the forward shocks, are shown in Figure 1. For this fictitious burst, current Imaging atmospheric Cherenkov telescopes would be more likely than space satellites such as EGRET, AGILE/GRID and *FGST*/LAT to detect the modeled emission, as seen in Figure 1.

4. VERY HIGH ENERGY AFTERGLOW EMISSION OF NEARBY GRBS

For photons with energy higher than ~ 100 GeV, the attenuation due to interaction with background photons is significant if the source has a high redshift. Therefore nearby bursts (those with $z < 0.25$) are chosen in this study.

4.1. The GRB Sample

To predict the VHE afterglow emission of nearby GRBs and compare the calculated results with sensitivity of different γ -ray telescopes, GRBs in our sample must satisfy: nearby events to alleviate the attenuation effect; at least two independent waveband low-energy afterglows are recorded to get relatively constrained parameters; the low-energy afterglow can be reproduced according to the afterglow model.

In this work, we consider nearby GRBs ($z < 0.25$) with relatively high luminosity and multi-wavelength afterglow data sufficient to meaningfully constrain the properties of the GRBs (i.e. the model parameter values as described in §2.1) up to March 2007. Five GRBs meet such criteria: GRB 030329, GRB 050509B, GRB 050709, GRB 060505, and GRB 060614. Though having a relatively large redshift of $z \sim 0.55$, GRB 051221A is also considered in this work because it is one of the brightest short GRBs detected so far.

GRB 030329 triggered the High Energy Transient Explorer, HETE-2 (Vanderspek et al. 2004). Very detailed BVRI afterglow light curves, spanning from ~ 0.05 to ~ 80 days, were compiled by Lipkin et al. (2004). Tiengo et al. (2004) reported XMM-Newton and Rossi XTE late-time observations of this burst. Based on the

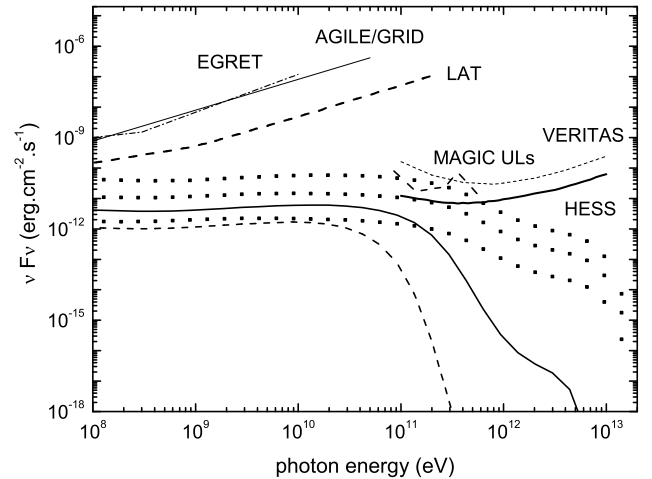


FIG. 1.— Temporal evolution of the observed high energy spectrum of SSC afterglows. The three dotted lines are the spectra at different epochs. All spectra, starting from (top) 0.5 hour, 2 hours, and (bottom) 10 hours, are integrated over 0.5 hour. They are calculated with the following parameter values: $E_0 = 5 \times 10^{51}$ erg, $\theta_0 = 0.4$, $n = 1.0 \text{ cm}^{-3}$, $p = 2.2$, $\epsilon_e = 0.3$, $\epsilon_B = 0.01$ and $z = 0.16$. The solid and dashed line are calculated with the same parameters represented above during the first epoch but occurring at larger redshift, $z = 0.5$ and $z = 1.0$, respectively. The sensitivity curves of EGRET (Thompson et al. 1993), AGILE/GRID (Galli & Guetta 2008), *FGST*/LAT (Galli & Guetta 2008), VERITAS (Horan et al. 2007) and HESS (assuming $\Gamma = 2.6$, Tam 2009) for an integration time of 0.5 hour are plotted as labeled. Magic 2-sigma upper limits derived from 30-min observations of GRB 060206 are also plotted, taken from Albert et al. (2007).

emission and absorption lines in the optical afterglow, a redshift of $z=0.1685$ has been identified (Greiner et al. 2003).

The X-Ray Telescope (XRT) onboard *Swift* began observations of GRB 050509B 62s after the trigger of the Burst Alert telescope (BAT) (Gehrels et al. 2005). Optical and infrared data were reported in Bloom et al. (2006). Prochaska et al. (2005) and Bloom et al. (2005) reported a redshift of $z \sim 0.22$ based on numerous absorption features and a putative host galaxy, respectively.

GRB 050709 was discovered by HETE-2 (Villasenor et al. 2005). Its prompt emission lasted 70 ms in the 3-400 keV energy band, followed by a weaker, soft bump of ~ 100 s duration. The optical counterpart of this burst was observed with the Danish 1.5-m telescope at the La Silla Observatory. The observations started 33 hours after the burst and spanned over the following 18 days (Hjorth et al. 2005). Observations with the Chandra X-ray observatory revealed a faint, uncatalogued X-ray source inside the HETE-2 error circle (Fox et al. 2005), which was coincident with a pointlike object embedded in a bright galaxy (Jensen et al. 2005) at $z = 0.16$ (Price et al. 2005).

GRB 051221A was localized by BAT (Cummings et al. 2005) and also simultaneously observed by the Konus-Wind instrument. The X-ray ($\sim 10^2 - 2 \times 10^6$ s;

Burrows et al. 2006) and the optical ($\sim 10^4 - 4 \times 10^5$ s; Soderberg et al. 2006) afterglow light curves of GRB 051221A were well detected, while in the radio band only one detection followed by several upper limits are available (Soderberg et al. 2006). Soderberg et al. (2006) detected several bright emission lines, indicating a redshift of $z = 0.5464$.

GRB 060505 was detected by BAT in the 15-150 keV band (Palmer et al. 2006; Hullinger et al. 2006). Ofek et al. (2006) reported the detection of the optical transient, later confirmed by VLT FORS2 observations (Thoene et al. 2006). XRT detected a source which was located about $4''$ from a galaxy with $z=0.0894$ (Conciatore et al. 2006).

GRB 060614 triggered both *Swift*-BAT (Parsons et al. 2006) and Konus-Wind (Golenetskii et al. 2006). XRT found a very bright (~ 1300 counts s^{-1}) un-catalogued source inside the BAT error circle. Ground-based optical and infrared follow-up observations were performed using several instruments (e.g., Cobb et al. 2006; Schmidt et al. 2006). Based on the detection of the host galaxy emission lines, a redshift of $z = 0.125$ was proposed by Price et al. (2006) and confirmed by Fugazza et al. (2006). Noted that the classification of GRB 060614 is ambiguous in the commonly-used long/short burst scheme, since it has a long duration but no accompanying SN (Gehrels et al. 2006; Fynbo et al. 2006).

4.2. Constraining the Model Parameters

The available multi-frequency afterglow data are then used to obtain the model parameters. In this work, we have reproduced the multi-frequency afterglow data of GRB 030329 and GRB 060614.

The well-sampled distinguishing afterglow behavior of GRB 030329 has gained much attention. Some authors concentrated on the rebrightening occurring at 1.6 days after the trigger and considered different mechanisms to explain the rebrightening features seen in the optical light curves (Huang et al. 2006). We concentrate on the multi-waveband emission, from radio (Berger et al. 2003), optical (Lipkin et al. 2004) to X-ray band (Tiengo et al. 2004) for the purpose in this paper. We show in Figure 2 that, with a certain set of parameters, the numerical results can describe the observed data in all three wavebands. Fluctuations were captured in *R* band afterglow light curves after 5×10^4 s from the burst trigger, which may imply the multiple energy injection into the outflow (Huang et al. 2006) or a two component jet (Berger et al. 2003). We ignore these details and focus on the general trend of the optical emission (particularly, in our calculation the energy of the relativistic ejecta is a constant). As shown in Figure 2, the difference is that in the time range $5 \times 10^4 - 10^5$ sec our approach gives a (little bit) brighter optical emission, so will be the high energy emission.

The modeled and observed afterglow light curves of GRB 060614 are shown in Figure 3. Energy injection, starting around 30 minutes after the GRB onset, is needed in the afterglow modeling to reproduce the increase in flux (instead of simple power-law decay seen in other GRBs). The early X-ray flux before 500s from the burst trigger, which is much brighter than the modeled

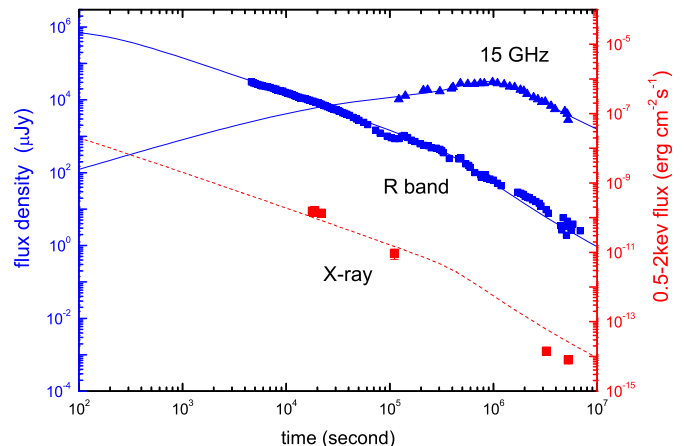


FIG. 2.— GRB 030329 afterglow data in the 15 GHz (Berger et al. 2003), *R*-band (Lipkin et al. 2004) and 0.5-2keV band (Tiengo et al. 2004). Symbols indicate data points as labelled. Solid lines represent the modeled *R*-band and 15 GHz emission (left plotting axis) and the dotted line represents the modeled X-ray emission (right plotting axis), respectively.

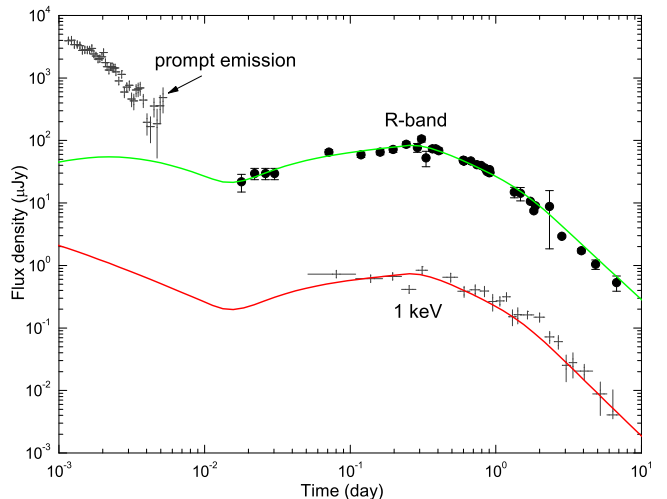


FIG. 3.— GRB 060614 afterglow data in the *R*-band and X-ray band (see also Xu et al. 2009). Crosses represent data recorded by *Swift*-XRT (0.2-10 keV), and circles represent *R*-band data. Solid and dashed lines represent the modeled *R*-band and 1 keV emission, respectively.

flux, results from the dominating contribution from the prompt emission.

Table 1 lists the physical parameters derived from the afterglow modeling for GRB 030329 and GRB 060614. Parameters of GRB 050509B, GRB 050709, GRB 051221A and GRB 060505 are taken from the literature, also listed in Table 1.

4.3. VHE Gamma-ray Observational Data

We are interested in VHE observations during the afterglow phase when the SSC is likely to dominate (see §5). VHE γ -ray afterglow data of three of the GRBs in the sample (i.e. GRB 030329, GRB 050509B, and GRB 060505) are available.

4.3.1. GRB 030329

Horan et al. (2007) reported a total of 4 hours of observations, which spanned five nights, using the Whipple 10-m telescope. No evidence for VHE γ -ray signal was found during any of the observation periods. When combining all data, a flux upper limit of $1.4 \times 10^{-11} \text{erg cm}^{-2} \text{s}^{-1}$ was derived. The first observation, lasting for about an hour, was started 64.6 hours after the burst. The 99.7% c.l. flux upper limit above an energy of ~ 400 GeV derived from this observation is shown in Table 2, as well as in Figure 4.

The 28-minute H.E.S.S. observation of GRB 030329 were taken 11.5 days after the burst (Tam et al. 2008). Since the burst position was located above the northern hemisphere, the zenith angle of the GRB observation was relatively large, i.e. 60° , resulting in an energy threshold of 1.36 TeV. No evidence for VHE γ -ray signal was found. The 99% c.l. flux upper limit (> 1.36 TeV) is $3.4 \times 10^{-11} \text{erg cm}^{-2} \text{s}^{-1}$, assuming a photon index of $\Gamma = 3$.

4.3.2. GRB 050509B

The observations of this burst using the STACEE detector employ an "on-off observation mode" and contain two 28-minute on/off pairs. The first on-source observation started 20 minutes after the burst and the second 80 minutes after the burst. After data quality cuts, about 18 minutes of useful on-source data remain in each observation. No evidence for VHE γ -ray signal above the energy threshold of 150 GeV was reported by Jarvis et al. (2008). The 95% c.l. flux upper limits (above 150 GeV, assuming a photon spectrum of $dN/dE \sim E^{-2.5}$) were $3.8 \times 10^{-10} \text{erg cm}^{-2} \text{s}^{-1}$ and $4.5 \times 10^{-10} \text{erg cm}^{-2} \text{s}^{-1}$ for the first and second on-source observation, respectively (A. Jarvis private communication).

4.3.3. GRB 060505

The H.E.S.S. observations began 19.4 hours after the burst and lasted for 2 hours (Tam et al. 2008). No evidence for VHE γ -ray signal was found. The 99% c.l. flux upper limit (> 0.45 TeV) is $8.8 \times 10^{-12} \text{erg cm}^{-2} \text{s}^{-1}$, assuming a photon index of $\Gamma = 3$.

4.4. Comparison to Observations

Based on the parameters obtained in §4.2, the GeV-TeV emission is obtained using the code described in §2.2.

We depict the calculated high energy afterglow spectrum in Figure 4, which shows the time-integrated high energy afterglow spectrum of these six events. The solid and dashed lines represent the intrinsic SSC spectra and corrected spectra for each GRB, respectively. The absorption is based on the cosmic infrared background model "P0.45" (Aharonian et al. 2006a)⁵. Such model

⁵ This implies a gamma ray horizon at a redshift of about 0.2 (0.05) for 500 GeV (10 TeV) gamma rays.

is constrained by the upper limits provided by two unexpectedly hard spectra of blazars at optical/NIR wavelengths and is close to the lower limit from integrated light of resolved galaxies.

In order to compare with the VHE observational data which are usually given in integrated photon fluxes, we integrate the spectra above the energy threshold. We consider first the GRBs with VHE data. These include GRB 030329, GRB 050509B, and GRB 060505. In Table 2 we list the modeled integrated energy fluxes after correction due to interaction with photons from cosmic infrared background, as well as the VHE γ -ray observations and the derived upper limits. All predicted fluxes are below the upper limits derived from the VHE observations.

We then investigate whether a sensitive VHE instrument is expected to detect the predicted VHE signal from nearby GRBs during the late afterglow phase. We use H.E.S.S. sensitivity as an example of an array of sensitive atmospheric Cherenkov telescopes. The sensitivity level of H.E.S.S. detector is shown in Figure 5, assuming a $\Gamma=2.6$ spectrum (Aharonian et al. 2006b). Assuming softer spectra, the level is higher, and the difference is about 50% between $\Gamma=2.0$ and $\Gamma=3.0$ (c.f. Aharonian et al. 2005). We show the temporal evolution of energy fluxes (>200 GeV) of six GRBs in our sample in Figure 5, indicating only the VHE signal from GRB 030329 may be above the H.E.S.S. sensitivity. For GRB 030329 which is a bright burst with low redshift, the expected energy flux would be high enough to be detected with a delayed observation time of $\lesssim 10$ hours if GRB position was favorable, i.e. with zenith angle $< 20^\circ$ (and thus an energy threshold of ~ 200 GeV is attained).

5. DISCUSSION

In this paper, we have calculated the SSC emission from the forward shock electrons following Fan et al. (2008). We shall discuss here the importance of other radiation processes in the late afterglow phase.

Possible VHE γ -ray emission initiated from protons has been suggested (Totani 1998; Böttcher & Dermer 1998). However, the proton-synchrotron component, as well as the hadron-related photo-meson electromagnetic components, is in most cases overshadowed by the SSC component of electrons in the afterglow phase. This is especially the case for the parameter values of ϵ_e and ϵ_B used here in the modeling of these six GRBs (e.g., Zhang & Mészáros 2001b).

Additional IC component will play a role and will enhance any VHE emission. SSC is, in general, only a lower limit. Another possible contribution to VHE emission is related to the "central engine afterglow" emission, like the flares (e.g., Falcone et al. 2007) or the plateaus followed by a sudden drop (e.g., Zhang 2009). The SSC radiation of the late internal shocks or the external inverse Compton radiation in the external forward shock front may be able to give rise to some VHE emission signals (see Fan & Piran 2008 for a review). However, no "central engine afterglow" emission has been reported in the late afterglow phase for the six bursts we studied. So it is hard for us to estimate its ability to enhance the detectability of the VHE emission.

As shown in Figure 5, we only expect detectable signal using a sensitive ground-based γ -ray detector for a

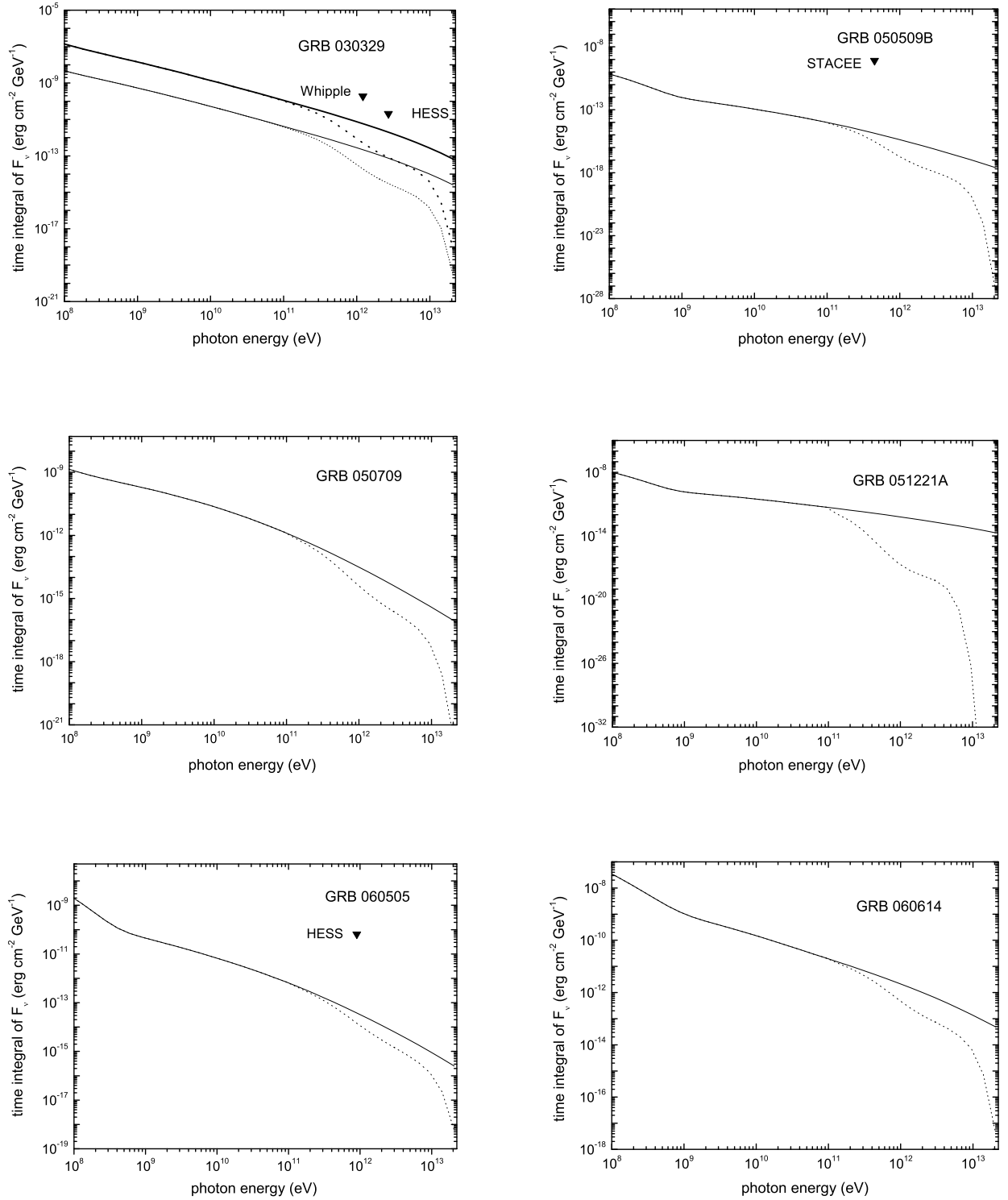


FIG. 4.— Modeled time-integrated 0.1 GeV – 20 TeV afterglow spectra of six GRBs, in comparison with VHE upper limits (triangles). Dotted and solid lines represent the spectra with and without correction by the cosmic infrared background, respectively. For GRB 030329, GRB 050509B, and GRB 060505, the spectra were integrated over the corresponding time intervals during which the upper limits were derived, as shown in Table 2. For GRB 030329, thick (upper) lines indicate the modeled spectrum for the Whipple observation time, and thin (lower) lines for the H.E.S.S. observation time. The data points are plotted at the corresponding average photon energies. The modeled spectra of the remaining three bursts are obtained by integrating the spectra over a time period of 2 hours, starting from 10 hours after the trigger.

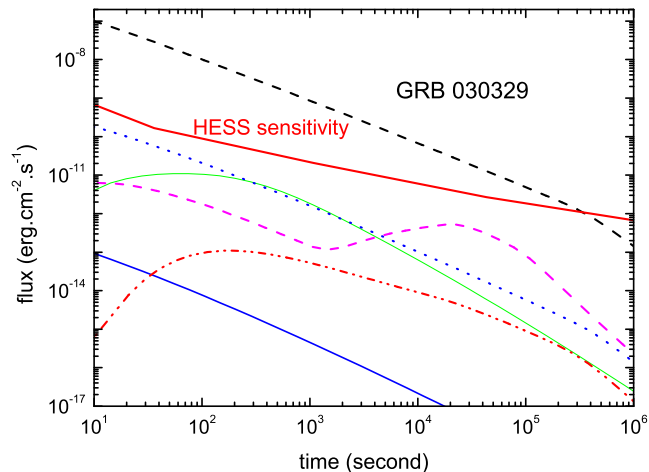


FIG. 5.— The temporal evolution of modeled VHE integral energy fluxes above 200 GeV for GRB 030329 (black dashed line), GRB 050509B (blue solid line), GRB 050709 (green solid line), GRB 051221A (red dash-dot-dotted line), GRB 060505 (blue dotted line) and GRB 060614 (magenta dashed line). The red solid line represents the HESS sensitivity if the observations start right at the GRB onset.

bright and nearby GRB like GRB 030329. The rate of such nearby and energetic GRBs is very uncertain. GRB 940217 might have been another event of this kind (Wei & Fan 2007).

Several factors that reduce the chance of detecting VHE photons can be summarized as follows: Firstly, as a result of large zenith angles (e.g., 60° for GRB 030329), the energy thresholds of some observations are relatively high (~ 1.4 TeV). Any VHE photon is severely attenuated by the cosmic infrared background, unless the level is very low. Secondly, the observations were taken at very late epochs, e.g. 11.5 days after the burst for H.E.S.S. observations of GRB 030329, when expected VHE flux had largely decayed. Thirdly, the fraction of low-redshift GRBs is small, e.g. see the catalogue in Butler et al. (2007). For GRB 051221A (at $z = 0.55$) studied here, the attenuation is severe at energies $\gtrsim 200$ GeV.

Despite these practical limitations, detection of VHE afterglow emission of GRBs is probable. Those GRBs close enough ($z < 0.5$) and with an intrinsic high luminosity (like GRB 030329), can be detected above ~ 200 GeV when the observation is taken within ~ 10 hours after the burst. From Eq. 1, GRBs with low z , large E_0 , large ϵ_e , and small ϵ_B are more likely to be detected in the VHE band. Besides, in general the expected VHE afterglow flux decays as $t^{-\alpha}$ where α is at least one. Thus, observations with shorter delay are more likely to probe the predicted VHE emission.

The main purpose of this work is to provide a relatively reliable prediction of the detectability of the VHE

emission from nearby GRBs. It is also interesting to explore the role of the VHE afterglow emission detection in revealing the GRB physics. Perhaps the most robust conclusion is that the VHE emission in late afterglow phase cannot be attributed to the synchrotron radiation of the forward shock, for which the maximal photon energy is $\approx 30\Gamma/(1+z)$ MeV (Cheng & Wei 1996), where Γ is the bulk Lorentz factor of the decelerating outflow. In general, for $\epsilon_B \geq \epsilon_e$, the inverse Compton emission is expected to be very weak. So the detection of VHE afterglow emission from GRBs requires that $\epsilon_B \ll \epsilon_e$, in support of the current radio/optical/X-ray afterglow modeling (e.g., see Tab.1). Together with *Swift*, *AGILE*, *FGST* and some ground-based optical telescopes, ground-based γ -ray detectors can provide us continuous spectra in the optical to TeV energy band during the afterglow phase. A self-consistent modeling of these data in a very wide energy band, in principle, will impose very tight constraint on the physical parameters and on the environment. However, given the small number of the VHE photons expected from a single burst, we do not expect that the VHE emission can help us a lot to achieve such goals.

6. CONCLUSIONS

In this work, we discuss the prospect of detecting VHE γ -rays with current ground-based detectors in the late afterglow phase. During this phase, the dominant radiation process in the VHE γ -ray regime is the SSC emission from the forward shock electrons. Klein-Nishina effects and attenuation by the cosmic infrared background, both known to suppress the VHE γ -ray spectra, were taken into account. To minimize the attenuation effect, we chose a sample of six nearby GRBs in this study. We have calculated the detailed SSC emission numerically using the model developed by Fan et al. (2008), with a set of parameters which are able to reproduce the available multi-wavelength afterglow light curves. The results are consistent with the upper limits obtained using VHE observations of GRB 030329, GRB 050509B, and GRB 060505. Moreover, assuming observations taken 10 hours after the burst, the VHE signal predicted from five GRBs is below the sensitivity level of a current sensitive atmospheric Cherenkov detectors mainly due to the low fluence of these outflows. For those bright and nearby bursts like GRB 030329, a VHE detection is possible even with a delayed observation time of ~ 10 hours.

We thank the anonymous referee for helpful comments and D. Xu for providing us data in Figure 3. This work is supported by the National Science Foundation (grants 10673034 and 10621303) and National Basic Research Program (973 programs 2007CB815404 and 2009CB824800) of China. YZF is also supported by a grant from Danish National Research Foundation. PHT acknowledges support from IMPRS-HD.

REFERENCES

- Aharonian, F., et al. (H.E.S.S. collaboration) 2005, *A&A*, 437, 135
 Aharonian, F., et al. (H.E.S.S. collaboration) 2006a, *Nature*, 440, 1018
 Aharonian, F., et al. (H.E.S.S. collaboration) 2006b, *A&A*, 457, 899
 Aharonian, F., et al. (H.E.S.S. collaboration) 2009, *A&A*, 495, 505
 Albert, J., et al. (MAGIC collaboration) 2007, *ApJ*, 667, 358

TABLE 1
MODEL PARAMETERS FOR SIX NEARBY GRBS

GRB	z	$E_0(\text{erg})$	θ_0	$n(\text{cm}^{-3})$	p	ϵ_e	ϵ_B	L_{eje}	q	injection timescale(s)	references
030329	0.1685	1.4×10^{53}	0.31	100	2.01	0.1	0.001	this work
050509B	0.2248	2.75×10^{48}	0.5	1	2.2	0.15	0.046	1
050709	0.16	3.77×10^{50}	0.5	6×10^{-3}	2.6	0.4	0.25	2
051221A	0.5465	10^{52}	0.1	0.01	2.4	0.3	2×10^{-4}	2×10^{48}	magnetar wind	$< 1.5 \times 10^4$	3
060505	0.089	2.6×10^{50}	0.4	1	2.1	0.1	0.008	4
060614	0.125	5×10^{50}	0.08	0.05	2.5	0.12	2×10^{-4}	10^{48}	0	$10^3 - 2 \times 10^4$	this work

REFERENCES. — 1 Bloom et al. (2006); 2 Panaitescu (2006); 3 Fan & Xu (2006); 4 Xu et al. (2009)

- Berger, E., et al. 2003, *Nature*, 426, 154
 Bloom, J., Blake, C., Prochaska, J. X., Hennawi, J., Gladders, M., & Koester, B. 2005, *GCN Circ.* 3386
 Bloom, J. S., et al. 2006, *ApJ*, 638, 354
 Böttcher, M. & Dermer, C. D. 1998, *ApJ*, 499, L131
 Burrows, D. N., et al. 2006, *ApJ*, 653, 468
 Butler, N. R., Kocevski, D., Bloom, J. S., & Curtis, J. L. 2007, *ApJ*, 671, 656
 Cheng, K. S., & Wei, D. M., 1996, *MNRAS*, 283, L133
 Cobb, B. E., Bailyn, C. D., van Dokkum, P. G., & Natarajan, P. 2006, *ApJ*, 651, L85
 Cohen, E., & Piran, T. 1999, *ApJ*, 518, 346
 Conciatore, M. L., Capalbi, M., Vetere, L., Palmer, D., & Burrows, D. 2006, *GCN Circ.* 5078
 Costa, E., et al. 1997, *Nature*, 387, 783
 Covino, S., et al. 2006, *A&A*, 447, L5
 Cummings, J., et al. 2005, *GCN Circ.* 4365
 Dai Z. G., & Lu T., 1998, *A&A*, 333, L87
 Dermer, C. D., Chiang, J., & Mitman, K. E. 2000 *ApJ*, 537, 785
 Falcone, A. D., et al. 2007, *ApJ*, 671, 1921
 Fan, Y. Z., & Piran, T., 2008, *Front. Phys. Chin.*, 3, 306
 Fan, Y. Z., Piran, T., Narayan, R., & Wei, D. M., 2008, *MNRAS*, 384, 1483
 Fan, Y. Z., & Xu, D. 2006, *MNRAS*, 372, L19
 Fox, D. B., Frail, D. A., Cameron, P. B., & Cenko, S. B. 2005, *GCN Circ.* 3585
 Fugazza, D., et al. 2006, *GCN Circ.* 5276
 Fynbo, J. P. U., et al., 2006, *Nature*, 444, 1047
 Galli, A., & Piro, L. 2007, *A&A*, 475, 421
 Galli, A., & Guetta, D. 2008, *A&A*, 480, 5
 Gehrels, N., et al. 2005, *Nature*, 437, 851
 Gehrels, N., et al. 2006, *Nature*, 444, 1044
 Golenetskii, S., Aptekar, R., Mazets, E., Pal'shin, V., Frederiks, D., & Cline, T. 2006, *GCN Circ.* 5264
 González, M. M., Dingus, B. L., Kaneko, Y., Preece, R. D., Dermer, C. D., & Briggs, M. S. 2003, *Nature*, 424, 749
 Gou, L. J., & Mészáros, P. 2007, *ApJ*, 668, 392
 Greiner, J., et al. 2003, *GCN*, 2020
 Hjorth, J., et al. 2005, *Nature*, 437, 859
 Horan, D., et al. 2007, *ApJ*, 655, 396
 Huang, Y. F., Gou, L. J., Dai, Z. G. & Lu, T. 2000, *ApJ*, 543, 90
 Huang, Y. F., Cheng, K. S., Gao, T. T. 2006, *ApJ*, 637, 873
 Hullinger, D., et al. 2006, *GCN Circ.* 5142
 Hurley, K., et al. 1994, *Nature*, 372, 652
 Jarvis, A., et al. 2008, *Proceedings of the 30th International Cosmic Ray Conference; Rogelio Caballero, Juan Carlos D'Olivio, Gustavo Medina-Tanco, Lukas Nellen, Federico A. Sánchez, José F. Valdés-Galicia (eds.); Universidad Nacional Autónoma de México, Mexico City, Mexico*, 3, 1111
 Jensen, B. L., et al. 2005, *GCN Circ.* 3589
 Kneiske, T. M., Mannheim, K., & Hartmann, D. H. 2002, *A&A*, 386, 1
 Lipkin, Y. M., et al. 2004, *ApJ*, 606, 381
 Mészáros, P., & Rees, M. J. 1994, *MNRAS*, 269, L41
 Mészáros, P., & Rees, M. J. 1997, *ApJ*, 476, 232
 Moderski, R., Sikora, M., & Bulik, T., 2000, *ApJ*, 529, 151
 Nousek, J. A., et al. 2006 *ApJ*, 642, 389
 Ofek, E. O., Cenko, S. B., Gal-Yam, A., Peterson, B., Schmidt, B. P., Fox, D. B., & Price, P. A. 2006, *GCN Circ.* 5123
 Omodei, N. 2008, *GCN Circ.* 8407
 Palmer, D., Cummings, J., Stamatikos, M., Markwardt, C., & Sakamoto, T. 2006, *GCN Circ.* 5076
 Panaitescu, A. 2006, *MNRAS*, 367, L42
 Parsons, A. M., et al. 2006, *GCN Circ.* 5252
 Price, P. A., Roth, K., & Fox, D. W. 2005, *GCN Circ.* 3605
 Price, P. A., Berger, E., & Fox, D. B., 2006, *GCN Circ.* 5275
 Primack, J. R., Somerville, R. S., Bullock, J. S., & Devriendt, J. E. G. 2001, *APIC Proc.*, 558, 463
 Prochaska, J. X., Bloom, J. S., Chen, H.-W., & Hurley, K. 2005, *GCN Circ.* 3399
 Rhoads, J. E., 1999, *ApJ*, 525, 737
 Roming, P. W. A., et al., 2006, *ApJ*, 652, 1416
 Rykoff E. S., et al., 2009, *ApJ* submitted (arXiv:0904.0261)
 Sari, R., Piran, T., & Narayan, R., 1998, *ApJ*, 497, L17
 Sari, R., Piran, T., & Halpern, J. P., 1999, *ApJ*, 519, L17
 Sari, R., & Esin, A. A. 2001, *ApJ*, 548, 787
 Schmidt, B., Peterson, B., & Lewis, K. 2006, *GCN Circ.* 5258
 Soderberg, A. M., et al. 2006, *ApJ*, 650, 261
 Stecker, F. W., Malkan, M. A., & Scully, S. T. 2006, *ApJ*, 648, 774
 Tajima, H., et al. 2008, *GCN Circ.* 8246
 Tam, P. H., Chadwick, P., Gallant, Y., Horns, D., Pühlhofer, G., Rowell, G., & Wagner, S. 2008, *Proceedings of the 30th International Cosmic Ray Conference; Rogelio Caballero, Juan Carlos D'Olivio, Gustavo Medina-Tanco, Lukas Nellen, Federico A. Sánchez, José F. Valdés-Galicia (eds.); Universidad Nacional Autónoma de México, Mexico City, Mexico*, 3, 1119
 Tam, P. H. 2009, Ph.D. Thesis, Ruprecht-Karls-Universität Heidelberg
 Tavani, M., Barbiellini, G., Argan, A., et al. 2008, [arXiv:0807.4254]
 Thoen, C. C., Fynbo, J. P. U., Sollerman, J., Jensen, B. L., Hjorth, J., Jakobsson, P., & Kloze, S. 2006, *GCN Circ.* 5161
 Thompson, D. J., et al. 1993, *ApJS*, 86, 629
 Tiengo, A., Mereghetti, S., Ghisellini, G., Tavecchio, F., & Ghirlanda, G. 2004, *A&A*, 423, 861
 Totani, T., 1998, *ApJ*, 502, L13
 Totani, T., & Takeuchi, T. T. 2002, *ApJ*, 570, 470
 Vanderspek, R., et al. 2004, *ApJ*, 617, 1251
 Villaseñor, J. S, et al. 2005, *Nature*, 437, 855
 Wang, X. Y., Dai, Z. G., & Lu, T. 2001, *ApJ*, 556, 1010
 Wei, D.M., & Lu, T., 1998, *ApJ*, 505, 252
 Wei, D.M., & Lu, T., 2000, *A&A*, 360, L13
 Wei, D.M., & Fan, Y. Z., 2007, *ChJAA*, 7, 509
 Xu, D., Starling, R. L. C., Fynbo, J. P. U., et al. 2009, *ApJ*, 696, 971
 Yu, Y. W., Liu, X. W., & Dai, Z. G. 2007, *ApJ*, 671, 637
 Zhang, B., & Mészáros, P. 2001a, *ApJ*, 552, L35
 Zhang, B., & Mészáros, P. 2001b, *ApJ*, 559, 110
 Zhang, B., Fan, Y. Z., Dyks, J., Kobayashi, S., Mészáros, P., Burrows, D. N., Nousek, J. A., & Gehrels, N. 2006, *ApJ*, 642, 354
 Zhang, X. H., 2009, *Research in Astronomy and Astrophysics*, 9, 213

TABLE 2
VHE GRB OBSERVATIONS AND MODEL PREDICTIONS

GRB	telescope	$T_{\text{OBS}} - T_{\text{GRB}}^{\text{a}}$	exposure	energy threshold (GeV)	energy flux upper limit set by observations ($\text{erg cm}^{-2} \text{s}^{-1}$)	predicted energy flux ($\text{erg cm}^{-2} \text{s}^{-1}$)	references
030329	H.E.S.S.	11.5 days	28 min	1360	3.4×10^{-11}	8.5×10^{-15}	1
030329	Whipple	64.55 hours	65.2 min	400	5.8×10^{-11}	6.7×10^{-13}	2
050509B	STACEE	20 min/80 min	28 min	150	$3.8 \times 10^{-10} / 4.5 \times 10^{-10}$	$2.2 \times 10^{-16} / 5.4 \times 10^{-17}$	3
060505	H.E.S.S.	19.4 hours	2 hours	450	8.8×10^{-12}	2.5×10^{-15}	1

REFERENCES. — 1 Tam et al. (2008); 2 Horan et al. (2007); 3 Jarvis et al. (2008)

^a The time between the start of the GRB and the beginning of observations for different telescopes.